Frontiers of Optoelectronics (2022) 15:47
https://doi.org/10.1007/s12200-022-00048-x

Frontiers of Optoelectronics

REVIEW ARTICLE

Copper-based metal halides for X-ray and photodetection

Fu Qiu[1] · Yutian Lei[1] · Zhiwen Jin[1]

Received: 19 July 2022 / Accepted: 29 August 2022

Abstract
Copper-based metal halides have become important materials in the field of X-ray and photodetection due to their excellent optical properties, good environmental stability and low toxicity. This review presents the progress of research on crystal structure/morphology, photophysics/optical properties and applications of copper-based metal halides. We also discuss the challenges of copper-based metal halides with a perspective of their future research directions.

Keywords Copper-based metal halides · X-ray detector · Photodetectors · Scintillators

1 Introduction

Lead-based metal halide has become a star material in the field of optoelectronic semiconductors due to its excellent optical properties such as high photoluminescence quantum yield (PLQY), tunable emission, and high absorption coefficient [1–5]. Different methods have been used to synthesize all-inorganic metal halides with different morphologies and to study their optical and physical properties. These metal halides have been widely used in solar cells [6–9], LEDs [10–12], photodetectors [13–16], scintillators [17–20] and lasers [21, 22]. However, their further development is hindered by the toxicity of the material.

To overcome the problem of lead (Pb) toxicity, the replacement of metal ions has achieved great success [23, 24]. The same or adjacent main group elements have similar chemical properties to lead, so replacing lead with germanium (Ge) [25], tin (Sn) [26], antimony (Sb) [27], and bismuth (Bi) [28] largely solves the problem of material toxicity. However, Sn^{2+} in Sn-based metal halides is easily oxidized to Sn^{4+} resulting in a significant reduction in the environmental stability of the material [29]. The optical properties of Sb-based and Bi-based metal halides need further enhancement to meet the application requirements [30]. Copper (Cu) is also used in metal ion replacement due to its large reserves, low price and low toxicity, etc.

In 2018, Jun et al. [31] first reported zero-dimensional (0D) $Cs_3Cu_2I_5$ with low toxicity, ultra-high PLQY, and tunable band gap. Low-dimensional copper-based metal halides are attracting attention due to high natural abundance, excellent photoelectric properties, and low toxicity. Compared with the classical three-dimensional (3D) $CsPbX_3$, the low-dimensional copper-based metal halides possess higher exciton binding energy and large Stokes shifts, and ultra-high PLQY; these properties make these materials promising in the field of X-ray and photodetection.

Here, we summarize the development status and existing problems of copper-based metal halides in terms of crystal structure, material morphology, physical properties, optical properties, and applications. At the end of this review, we discuss the challenges of all-inorganic copper-based metal halides and the prospects for future research directions.

2 Crystal structure and morphology

2.1 Crystal structure

Different kinds of crystal structures determine different electronic properties of materials [32]. Copper elements of different valencies combine with different halogen atoms to form various crystal structures. The crystal structures of copper-based metal halides have been studied from as early as 2004 [33]. Figure 1 shows the schematic crystal structures of three typical all-inorganic copper-based metal halides

✉ Zhiwen Jin
jinzw@lzu.edu.cn

[1] School of Physical Science and Technology & Key Laboratory for Magnetism and Magnetic Materials of Ministry of Education, Lanzhou University, Lanzhou 730000, China

Published online: 21 November 2022

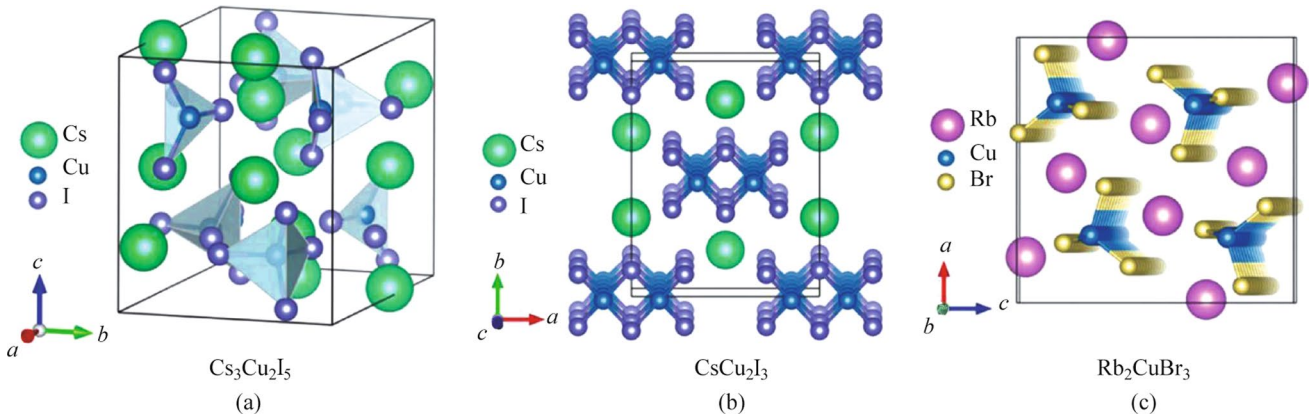

Fig. 1 Crystal structures of copper-based metal halides: **a** $Cs_3Cu_2I_5$; **b** $CsCu_2I_3$; **c** Rb_2CuBr_3. Reprinted with permission from Ref. [34], Copyright 2021, Royal Society of Chemistry

[34]. To be specific, $Cs_3Cu_2I_5$ belongs to a typical 0D crystal structure (Fig. 1a). Two types of Cu^+ sites, trihedral site and tetrahedral site, are present in this crystal structure. Each site is composed of $[Cu_2I_5]^{3-}$ which is separated by Cs^+ to form the 0D crystal structure [31]. It is worth noting that there are differences in the space group of $Cs_3Cu_2X_5$ (X = Cl, Br and I), with $Cs_3Cu_2Cl_5$ belonging to *Cmcm* and the remaining two belonging to *Pmpm* [35]. On the other hand, $CsCu_2I_3$ is a typical one-dimensional (1D) crystal structure (Fig. 1b). It belongs to the *Cmcm* space group. Cu^+ combines with the surrounding I^- to form $[Cu_2I_3]^-$ tetrahedra. The tetrahedra are separated by Cs^+, and each tetrahedron extends in a co-edge manner to form 1D $[Cu_2I_3]^-$ anionic chains [36]. Besides, Rb_2CuBr_3 also belongs to 1D crystal structure but in the space group *Pnma* (Fig. 1c). The $[CuBr_3]^{2-}$ tetrahedra separated by Rb^+ extends in a co-angular manner to form one-dimensional long chains of anions $[CuBr_3]^{2-}$ [37].

2.2 Morphology

In recent years, as the understanding of copper-based metal halides has improved, copper-based metal halides with different morphological dimensions have been successfully prepared [19, 32, 38]. It can be mainly divided into single crystals, polycrystalline powder, thin film, and nanocrystals. Materials with different morphologies can be obtained by different ingenious preparation methods [20, 39, 40].

Single crystals with a certain size can be prepared by antisolvent vapor-assisted crystallization and inverse temperature crystallization. The principle of antisolvent vapor-assisted crystallization is based on the different solubility of metal halide precursors in various solvents to grow single crystals. The slow diffusion of antisolvent vapors into the saturated precursor solution contributes to the slow growth of single crystals, but this method has a long growth time cycle. If the solubility of metal halides is low at higher temperatures, the inverse temperature crystallization method can also be adopted to grow single crystals. This method is simpler and faster than the antisolvent vapor-assisted crystallization method.

Polycrystalline powders can be synthesized by high-temperature sintering techniques and ball milling methods. In both methods, the stoichiometric ratios between the reaction materials can be adjusted to obtain products of different components and the synthetic yields are much higher than those of other methods. However, the ease of reaction of the raw materials is highly required. In general, the easier the reaction between the raw materials, the more suitable these two methods are.

Spin coating is the classic and most commonly used preparation method for thin films. The introduction of antisolvent engineering in the process of film spin coating has greatly improved film quality. Nanocrystals can be synthesized by hot injection method and antisolvent recrystallization. In the hot injection method, different sizes of nanocrystals can be prepared by adjusting the temperature. The size of nanocrystals affects the optical properties of the material, and there is a big difference in the optical properties between materials with different sizes of nanocrystals. This is one of the advantages of quantum dot materials.

Copper-based metal halides with different morphologies have different physical properties and different applications, as shown in Fig. 2, so their development status will be presented respectively.

2.2.1 Single crystals

In single crystal materials, the crystal cells are regularly and periodically arranged in three-dimensional space, and the entire crystal exhibits a long-range ordered nature in space. So, single crystal material has many excellent physical properties, such as high carrier mobility, low defect density, good

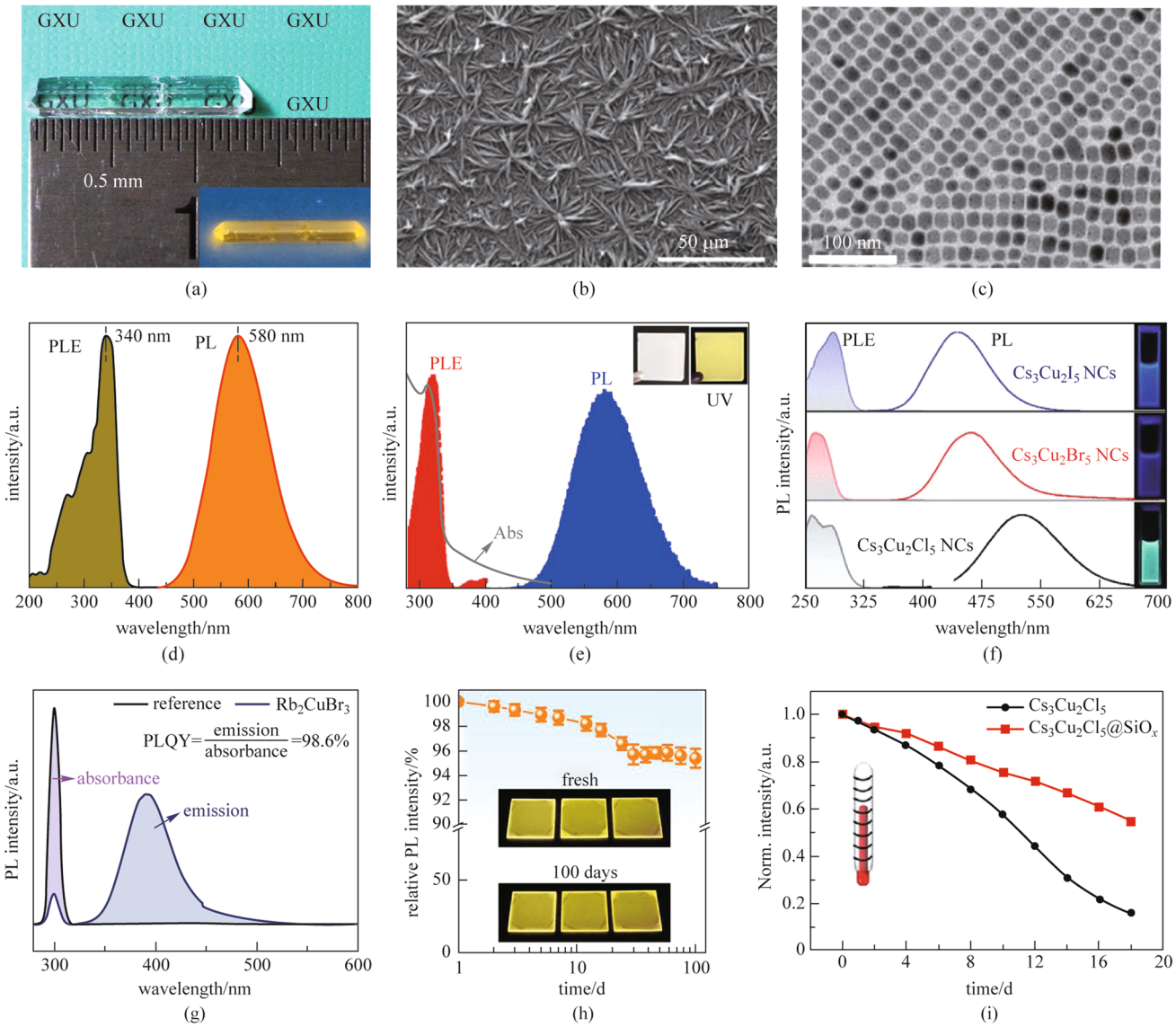

Fig. 2 **a** Photographs of $CsCu_2I_3$ single crystals under ambient light and 365 nm UV light (inset). Reprinted with permission from Ref. [44], Copyright 2021, ELSEVIER; **b** SEM image of $CsCu_2I_3$ film. Reprinted with permission from Ref. [46], Copyright 2020, American Chemical Society; **c** TEM image of $Cs_3Cu_2I_5$ nanocrystal. Reprinted with permission from Ref. [52], Copyright 2020, WILEY–VCH Verlag GmbH; **d** PLE and PL spectrum of $CsCu_2I_3$ single crystals. Reprinted with permission from Ref. [44], Copyright 2021, ELSEVIER; **e** Light absorption (gray), PLE (red), and PL (blue) spectrum of the $CsCu_2I_3$ film. Insets present the bright-field (left) and fluorescence photographs (right). Reprinted with permission from Ref. [46], Copyright 2020, American Chemical Society; **f** PLE and PL spectrum of $Cs_3Cu_2X_5$ nanocrystal solutions. Right insets show the photographs of $Cs_3Cu_2X_5$ nanocrystal solutions under 254 nm UV light. Reprinted with permission from Ref. [52], Copyright 2020, Wiley–VCH Verlag GmbH; **g** PLQY spectrum of Rb_2CuBr_3 crystals. Reprinted with permission from Ref. [37], Copyright 2019, WILEY–VCH Verlag GmbH; **h** PL intensity evolution of the $CsCu_2I_3$ thin films measured at different storage periods in ambient air. The insets present the photographs of the $CsCu_2I_3$ thin films under UV light excitation before and after storage for 100 days. Reprinted with permission from Ref. [47], Copyright 2020, American Chemical Society; **i** Normalized PL intensity of $Cs_3Cu_2Cl_5$ nanocrystals and $Cs_3Cu_2Cl_5$@SiO_x nanocrystals during a heat treatment at 80 °C. Reprinted with permission from Ref. [53], Copyright 2021, WILEY–VCH Verlag GmbH

environmental stability. $Cs_3Cu_2X_5$ single crystals with 0D crystal structure have shown excellent optical properties and have been intensively studied. In 2018, Jun et al. [31] reported for the first time that a $Cs_3Cu_2I_5$ single crystal was prepared by vapor antisolvent method. It was shown to have a photoluminescence (PL) peak at 445 nm with a high PLQY of 90%. The high PLQY means it has potential applications in the field of LEDs or scintillators. In 2020, Zhang et al. [41] successfully prepared $Cs_3Cu_2I_5$ single crystals with millimeter size by the room temperature solvent evaporation crystallization method. In the same year, Lin et al. [42] prepared $Cs_3Cu_2I_5$ single crystals with PLQY ≈ 100% by the

antisolvent vapor-assisted crystallization method. They suggested that the $Cs_3Cu_2I_5$ single crystal had a near-uniform PLQY thanks to its unique 0D crystal structure. Due to the excellent PLQY performance, they applied the material to LEDs. In 2021, Zhou et al. [43] prepared $Cs_3Cu_2X_5$ (X = Cl, Br or mixed Br/Cl) single crystals by the rapid cooling crystallization method. The PLQY of these materials is ~ 100% at 525 nm, and 27% at 462 nm for X = Cl and Br respectively. They further investigated the effect of different halogen combinations on the luminescence properties of the material and found that the tunability of the luminescence wavelength can be achieved by changing the ratio of Cl^- to Br^-.

In addition, $CsCu_2X_3$ and A_2CuX_3 (A = Rb or K, X = Cl or Br) with one-dimensional electronic structures have also attracted attention from scientists. In 2019, Lin et al. [36] successfully prepared $CsCu_2I_3$ single crystals with a size of 10 mm × 1.5 mm by the antisolvent infiltration method and applied them to white LEDs. It was shown to have a PL peak at 568 nm with a PLQY of 15.7%. In 2021, Mo et al. [44] have synthesized and demonstrated $CsCu_2I_3$ single crystals with lengths as long as 13 mm by using the inverse temperature crystallization method, as shown in Fig. 2a. The crystals showed a large Stokes shift with a photoluminescence excitation (PLE) peak at 340 nm and a PL peak at 580 nm (Fig. 2d). They used oleic acid as an additive in the process of crystal growth to increase PLQY to 50% for the first time. Replacement A-site ions have been demonstrated and widely used to improve the optical properties and the environmental stability of the material. By comparison, it is interesting to note that the PLQY of $Cs_3Cu_2I_5$, which possesses a 0D structure, is significantly higher than that of $CsCu_2I_3$, which possesses a 1D structure. The reason is that the exciton binding energy of 0D $Cs_3Cu_2I_5$ is much higher than that of 1D $CsCu_2I_3$, and the exciton binding energy affects the PL performance of the material at room temperature. In 2019, Yang et al. [37] successfully prepared Rb_2CuBr_3 single crystals by the slow cooling method. Rb_2CuBr_3 exhibits superior optical properties to $CsCu_2I_3$. It was shown to have a PL peak at 385 nm with a PLQY of 98.6%, as shown in Fig. 2g. They also demonstrated application of this single crystal in X-ray scintillators and showed superior light yield (the light yield of ~ 91,056 photons per MeV) compared to traditional materials. In 2020, Zhao et al. [45] prepared Rb_2CuCl_3 single crystals using the slow cooling method. Rb_2CuCl_3 exhibits violet emission at 397 nm with a PLQY of 99.4% and has a light yield of 16,600 photons per MeV. The material shows its potential applications in the field of high-energy X-ray detection.

Although the single crystal has many excellent physical properties, its complicated preparation process and the impossibility of preparing large areas limit its development. Therefore, the search for a simple and high-quality preparation method is a huge problem for copper-based metal halides.

2.2.2 Thin film and polycrystalline powder

The physical properties of thin films are not as good as those of single crystals. However, the preparation cycle of the thin film is shorter than that of the single crystals and the thin film can be prepared in a large area and are flexible. In 2020, Yang et al. [46] successfully prepared $CsCu_2I_3$ thin films by the antisolvent-assisted crystallization method. From the SEM image (Fig. 2a), it is clear that the quality of $CsCu_2I_3$ film needs to be further optimized. It was shown to have a PL peak at 580 nm with a PLQY of 12.3%, as shown in Fig. 2e. In the same year, Ma et al. [47] prepared $CsCu_2I_3$ thin films by the spin-coating method and applied them to yellow LEDs. The PLQY of the thin film was increased to 20.6% by using anti-solvent engineering. The film showed excellent stability against oxygen, moisture, and heat, as shown in Fig. 2h.

The preparation of copper-based metal halides by solution spin-coating faces a serious problem, namely the insolubility of the raw material and in turn the poor film quality. The quality of the precursor solution largely determines the quality of the film during the preparation of the film by the solution method. To avoid this problem, some groups have turned their attention to solid-phase reaction methods that do not require solutions. The solid-phase reaction completely solves the insolubility problem of raw materials and the preparation process is simpler. In 2019, Roccanova et al. [48] successfully synthesized $Cs_3Cu_2Br_{5-x}I_x$ ($0 \le x \le 5$) polycrystalline powder by a solid-phase reaction. The PLQY increase linearly with x from 50.1% for $Cs_3Cu_2Br_5$ to 98.7% for $Cs_3Cu_2I_5$. In 2020, Grandhi et al. [35] prepared high-quality phase-pure $Cs_3Cu_2X_5$ polycrystalline powders by an all-solid-state mechanochemical synthesis method. They focused on the structural transformation of the raw materials with different stoichiometric ratios in solid-phase reactions. For example, the amount of CsI affects the phase transition between $Cs_3Cu_2I_5$ and $CsCu_2I_3$. The chemical reaction of 4 mol of CsI with 1 mol of $Cs_3Cu_2I_5$ produces 3 mol of $CsCu_2I_3$. In this process, the isolated $[Cu_2I_5]^{3-}$ units of $Cs_3Cu_2I_5$ are transformed into double chains of $[Cu_2I_3]^-$. This transformation process can be reversed by the addition of CsI to $CsCu_2I_3$. The transformation of the crystal structure from 1D to 0D causes a great change in the luminescence performance, which can be achieved by electronic structure design. In 2020, Xie et al. [49] used the ball milling method to synthesize $Cs_3Cu_2X_5$ with PLQY up to 60%. The blue emissive $Cs_3Cu_2I_5$ and green emissive $Cs_3Cu_2Cl_5$ polycrystalline powders obtained have good thermal stability and photostability.

Although copper-based metal halide thin films and polycrystalline powders have achieved relatively good research results, they still face some serious problems, such as non-uniform films, and poor film quality.

2.2.3 Nanocrystals

In 2019, Cheng et al. [50] successfully prepared 1D $CsCu_2I_3$ nanorods and 0D $Cs_3Cu_2I_5$ nanocrystals by the hot injection method. They found that the reaction temperature was an important factor affecting the final product in the preparation. When the reaction temperature was 110 °C, the end product was $CsCu_2I_3$, and when the reaction temperature was 70 °C, the end product was $Cs_3Cu_2I_5$. They also found that $CsCu_2I_3$ was not stable in solution and tended to form nanorods. In 2020, Li et al. [51] synthesized $Cs_3Cu_2X_5$ (X = I, Br/I, Br, Br/Cl and Cl) nanocrystals at room temperature by the antisolvent method. These nanocrystals have uniform sizes of less than 10 nm in diameter and show excellent optical properties, including composition-tuned emission spectrum over the spectral region of 440 − 530 nm, and with high PLQY of ~100%, 20%, and 30% for X = Cl, Br, and I, respectively. In 2020, Luo et al. [52] prepared $Cs_3Cu_2X_5$ nanocrystals by the hot-injection method, as shown in Fig. 2c. These $Cs_3Cu_2X_5$ nanocrystals exhibited broadband blue-green photoluminescence emissions in the range of 445–527 nm with large Stokes shifts, as shown in Fig. 2f. It is worth paying attention to the PL emissions of $Cs_3Cu_2X_5$ nanocrystals, which are quite different from those of typical $CsPbX_3$ nanocrystals. $CsPbX_3$ nanocrystals show a blueshift via successive substitution of X halogen ion from I^- to Br^-, and then to Cl^-, while $Cs_3Cu_2X_5$ show redshift by successive substitution of X-halogen ions from I^- to Br^-, and then to Cl^-. The reason for this phenomenon is the unique self-trapped exciton (STE) luminescence behavior of copper-based metal halides. For STE emission, the emission energy is not only related to the bandgap, but also depends on the exciton binding energy, lattice distortion energy and self-trapping energy. In addition, $Cs_3Cu_2Cl_5$ nanocrystals have the relatively best luminescence performance with a PLQY of 48.7%. $Cs_3Cu_2I_5$ nanocrystals exhibit considerable air stability over 45 days.

Among the studies on copper-based metal halides, $Cs_3Cu_2Cl_5$ nanocrystals have attracted much attention due to their excellent luminescence properties. To further improve their luminescence properties and stability, Zhao et al. [53] optimized $Cs_3Cu_2Cl_5$ nanocrystals by encapsulating. They coated $Cs_3Cu_2Cl_5$ nanocrystals with SiO_x shells to increase the PLQY of $Cs_3Cu_2Cl_5$ nanocrystals to 76%. Due to the presence of SiO_x shells, $Cs_3Cu_2Cl_5$ nanocrystals have improved stability against water, moisture, and heat. $Cs_3Cu_2Cl_5@SiO_x$ nanocrystals show potential for luminescence applications due to their excellent luminescence properties and environmental stability, as shown in Fig. 2i.

For a better comparison, the differences between the optical properties of copper-based metal halides with different morphologies are summarized in Table 1.

3 Photophysics and optical properties

3.1 Photophysics

Most properties (such as charge transfer and optical properties) of metal halide systems are determined by their electronic structures, including the spatial and energy distribution of electrons. To date, the band structures, the projected density of states (PDOSs), and many other electronic properties of copper-based metal halides have been studied extensively. The typical electronic structures and PDOSs of copper-based metal halides are shown in Fig. 3.

$Cs_3Cu_2Cl_5$ is a direct bandgap semiconductor with both the conduction band minimum (CBM) and valence band maximum (VBM) being located at the Γ point, as shown in Fig. 3a. The theoretical calculation shows that the bandgap is 3.70 eV, which is not much different from the experimental measurement of 3.65 eV. From knowledge of PDOSs we can understand the electronic orbital structure of $Cs_3Cu_2Cl_5$ more intuitively and deeply. We can see that the VBM is mainly composed of Cu 3d and Cl 4p orbitals, whereas the CBM consists of both Cu 4 s and Cl 3p orbitals [54]. Cs is not involved in the composition of these electron orbitals, and electrons and holes are mainly concentrated on Cu and Cl, as shown in Fig. 3b. This corresponds to the crystal structure of $Cs_3Cu_2Cl_5$. It is noteworthy that the exciton binding energy of copper-based metal halides is much greater than that of lead-based metal halides. The exciton binding energy of $Cs_3Cu_2Cl_5$ is about 553.55 meV resulting in higher stability and enhanced PL emission at room temperature. The Huang-Rhys factor of the $Cs_3Cu_2Cl_5$ films is 26.21 which indicates that $Cs_3Cu_2Cl_5$ has a soft crystal lattice, where the excitons are easily self-trapped and generate STE emissions [55]. Figure 3c, d shows the first-principles calculation results of $CsCu_2I_3$. In the energy band diagram, $CsCu_2I_3$ has a direct band gap and a theoretically calculated band gap of 2.05 eV, with a low density of states at CBM and a flat density of states at VBM. From the state density, the VBM is mainly composed of Cu 3d and I 5p orbitals, while the CBM mainly contains Cu 4 s and I 5p orbitals. The Cs contribution to VBM and CBM is too small to be considered [36]. The exciton binding energy of $CsCu_2I_3$ is about 346.23 meV and the Huang-Rhys factor of the $CsCu_2I_3$ is 19.84 [36]. Such high exciton binding energy comes from its unique one-dimensional electronic structure. The Cu–I

Table 1 Summary of optical parameters of copper-based metal halides

Formula	Morphology	Method	PL/nm	PLQY/%	Ref.
$Cs_3Cu_2I_5$	Single crystal	Vapor antisolvent method	445	90	[31]
$Cs_3Cu_2I_5$	Single crystal	Solvent evaporation crystallization method	442	89	[41]
$Cs_3Cu_2I_5$	Single crystal	Antisolvent vapor-assisted crystallization method	443	~100	[42]
$Cs_3Cu_2Br_5$	Single crystal	Rapid cooling crystallization method	462	27	[43]
$Cs_3Cu_2Cl_5$	Single crystal		525	~100	
$CsCu_2I_3$	Single crystal	Antisolvent infiltration method	568	15.7	[36]
$CsCu_2I_3$	Single crystal	Inverse temperature crystallization method	580	50	[44]
Rb_2CuBr_3	Single crystal	Slow cooling method	385	98.6	[37]
Rb_2CuCl_3	Single crystal	Slow cooling method	397	99.4	[45]
$CsCu_2I_3$	Film	Antisolvent-assisted crystallization method	580	12.3	[46]
$CsCu_2I_3$	Film	Spin-coating method	548	20.6	[47]
$Cs_3Cu_2I_5$	Powder	Solid-phase reaction	443	98.7	[48]
$Cs_3Cu_2Br_5$	Powder		454	50.1	
$Cs_3Cu_2I_5$	Powder	All-solid-state mechanochemical synthesis method	440	62	[35]
$Cs_3Cu_2Br_5$	Powder		460	10	
$Cs_3Cu_2Cl_5$	Powder		525	60	
$Cs_3Cu_2I_5$	Powder	Ball milling method	440	60	[49]
$Cs_3Cu_2Cl_5$	Powder		510	53	
$CsCu_2I_3$	Nanorods	Hot injection method	553	5	[50]
$Cs_3Cu_2I_5$	Nanocrystals		441	67	
$Cs_3Cu_2I_5$	Nanocrystals	Room temperature antisolvent method	443	30	[51]
$Cs_3Cu_2Br_5$	Nanocrystals		458	20	
$Cs_3Cu_2Cl_5$	Nanocrystals		521	~100	
$Cs_3Cu_2I_5$	Nanocrystals	Hot injection method	445	29.2	[52]
$Cs_3Cu_2Br_5$	Nanocrystals		461	16.9	
$Cs_3Cu_2Cl_5$	Nanocrystals		527	48.7	
$Cs_3Cu_2Cl_5@SiO_x$	Nanocrystals	Hot-injection method	523	76	[53]

octahedron providing electronic state is strongly isolated by Cs atoms along 1D direction, which strengthens the localization of exciton. The electronic structure of Rb_2CuBr_3 is similar to that of CsCu2I3. Figure 3e, f shows the electronic energy band structure and the PDOSs of Rb_2CuBr_3. It is a direct band gap semiconductor with a bandgap of 3.51 eV at the Γ point. It is evident from the energy band diagram that the density of states at the CBM is low, while it is relatively flat at the VBM. The PDOSs indicates that the CBM of Rb_2CuBr_3 is primarily composed of Cu 4 s, Br 4 s, and Br 4p orbitals, whereas the VBM consists of Br 4p and Cu 3d orbitals, and Rb does not contribute to CBM or VBM [37]. The exciton binding energy of Rb_2CuBr_3 is about 758.87 meV and the Huang-Rhys factor of the Rb_2CuBr_3 films is 37.17 [37].

3.2 Optical properties

Copper-based metal halides are dominated by 0D and 1D crystal structures, and their low-dimensional crystal structures possess strong electron–phonon coupling. In addition, the crystal structure is easily distorted under external stimulation, such as UV and X-ray excitation. These special crystal structure characteristics contribute to the unique photophysics/optical properties of copper-based metal halides. Most copper-based metal halides were reported to exhibit wide full width at half maxima (FWHM), large Stokes shifts as well as long lifetimes, which can be attributed to STE emission.

As a classical phenomenon originating from soft lattices and strong electron–phonon coupling, STE luminescence has been intensively studied in many fields. Under the effect of photoexcitation, the strong electron–phonon coupling leads to lattice distortion. Due to the lattice distortion, electrons and holes are separated in space to form a stable self-trapped exciton state. This self-trapped exciton state has a smaller band gap and stronger localization effect than the original state. Finally, the material will exhibit optical properties of broad-spectrum, large Stokes shift and long lifetime (Fig. 4) [56, 57]. The contribution of A-site ions to the material properties was found to be very small in the studies of the crystal structure and energy bands of

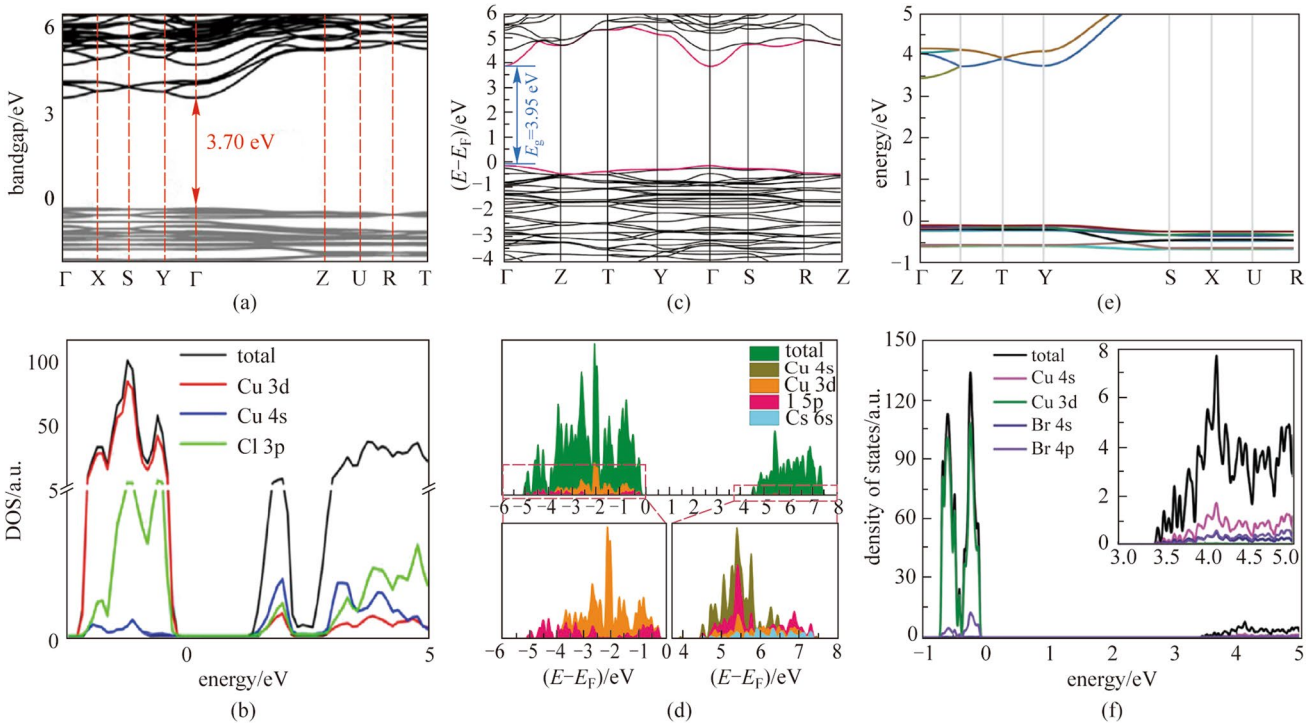

Fig. 3 Electronic properties of $Cs_3Cu_2Cl_5$: **a** Electronic band structure, **b** PDOSs. Reprinted with permission from Ref. [54], Copyright 2020, WILEY–VCH Verlag GmbH; Electronic properties of $CsCu_2Cl_3$: **c** Electronic band structure, **d** PDOSs. Reprinted with permission from Ref. [36], Copyright 2021, ELSEVIER; Electronic properties of Rb_2CuBr_3: **e** Electronic band structure, **f** PDOSs. Reprinted with permission from Ref. [37], Copyright 2019, WILEY–VCH Verlag GmbH

copper-based metal halides. Therefore, the optical properties of copper-based metal halides are mainly influenced by the interaction between copper atoms and halogens. The optical properties of both $Cs_3Cu_2X_5$, which has a 0D structure, and $CsCu_2X_3$ and A_2CuX_3, which have a 1D structure, can be attributed to STE. Next, $Cs_3Cu_2I_5$ is used as an example to deeply understand the principle of STE. The PLE and PL peak wavelengths are 290 and 445 nm, respectively, as shown in Fig. 4a. A large Stokes shift of ~ 155 nm is similar to those of other 0D metal halides. In addition, the exciton binding energy evaluated for $Cs_3Cu_2I_5$ was ~ 490 meV and the exciton lifetime of $Cs_3Cu_2I_5$ was ~ 464 ns, which is much larger than that of the 3D metal halides, as shown in Fig. 4b, c. The main reason for these properties is the excited-state structural reorganization. Under photoexcitation conditions, the Cu(I)-3d10 electron orbital is distorted to form the Cu(II)-3d9. The change of electron orbital configurations leads to the reorganization of the excited state structure, while the Stokes shift depends mainly on the energy difference between the excited states, i.e., between Cu(I)-3d10 and Cu(II)-3d9. In addition, the strong electron–phonon coupling leads to the deformation of the lattice, resulting in the spatial separation of electrons from holes. Therefore, the carrier recombination process is spatially suppressed leading to a long exciton lifetime [31]. In conclusion, we can understand the STE luminescence mechanism from the molecular orbital theory, as shown in Fig. 4d. When the material is in an excited state, Cu(I)-3d10 is deformed into Cu(II)-3d9, which produces the Jahn–Teller effect and changes the energy level distribution of the excited state.

4 Applications

4.1 Photodetectors

With the various needs of society, high performance UV detectors is becoming more and more in demand. Owing to their excellent optical properties in UV regions, copper-based metal halides have gained wide application in the field of UV detection as shown in Fig. 5.

In 2019, Zhang et al. [58] first reported a deep-ultraviolet photodetector made up of $Cs_3Cu_2I_5$. They prepared a planar structured UV detector with $Cs_3Cu_2I_5$ film deposited on ITO glass by the method of slow vapor saturation of an antisolvent. The UV detector shows high sensitivity to deep UV light at 265 nm. Specifically, at 1 V, the responsivity, detectivity, and external quantum efficiency (EQE) were 64.9 mA/W, 6.9×10^{11} Jones, and 0.3%, respectively. In 2020, Li et al. [59, 60] successfully prepared $Cs_3Cu_2I_5$/GaN

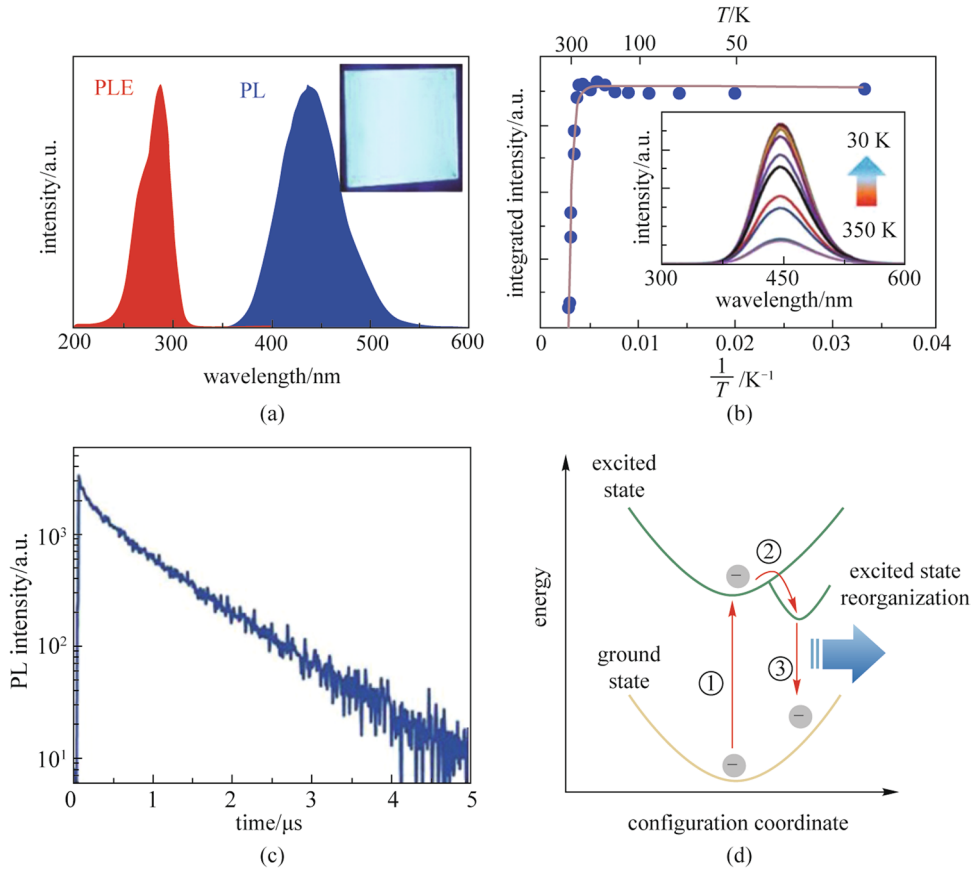

Fig. 4 Optophysical properties of $Cs_3Cu_2I_5$: **a** PL and PLE spectrum of the $Cs_3Cu_2I_5$ thin film; **b** Integrated PL intensity as a function of reciprocal temperature from 30 to 350 K. The inset of **b** shows the temperature-dependent PL spectrum; **c** Time-resolved PL decay curve at room temperature; **d** Mechanism of configuration coordinate for the excited-state reorganization. Reprinted with permission from Ref. [31], Copyright 2018, WILEY–VCH Verlag GmbH

heterojunctions (Fig. 5a) to achieve selective detection in the 300–370 nm. The photodetectors demonstrate a high responsivity of 0.28 A/W, a specific detectivity of 1.4×10^{12} Jones (Fig. 5b), an on/off photocurrent ratio of 1.2×10^{5}, and fast response speeds of 95 (rise time)/130 (fall time) μs under UV light excitation (320 nm). In addition, the device exhibits excellent operating stability in open air environments, as shown in Fig. 5c. In the same year, they also discovered that $CsCu_2I_3$ nanowires possess polarized UV detection capabilities due to the intrinsic anisotropy of their asymmetric structure and the anisotropy of their external morphology. They prepared $CsCu_2I_3$ nanowires as polarization-sensitive UV detectors, and the devices obtained a photoresponsivity of 32.2 A/W, a specific detectivity 1.89×10^{12} Jones, and response speeds of 6.94 (rise time)/214 (fall time) μs. They also prepared devices with flexible substrates, which have good flexibility and stability, with almost no degradation of performance after 1000 bending cycles. In 2021, Ma et al. [61] prepared a $Cs_3Cu_2I_5$/β-Ga_2O_3 heterojunction and applied it to a solar-blind UV photodetector. This photodetector exhibits a low dark current of 1.2 pA, a high photoresponsivity of 2.3 mA/W, and a high on/off ratio of ~5.1×10^{4} at zero bias, under 265 nm light illumination.

Overall, copper-based metal halides are promising candidates for low-cost, high-performance UV photodetectors.

4.2 X-ray scintillators

All-inorganic copper-based metal halides are also attracting attention in the field of scintillators due to their large Stokes shift and high PLQY as shown in Fig. 5.

In 2019, Yang et al. [37] used Rb_2CuBr_3 as an X-ray scintillator, which exhibited excellent performance. The light yield of 91,056 photons per MeV was much higher than that of traditional scintillators. In 2020, Zhao et al. [45] studied the photovoltaic properties of Rb_2CuCl_3 materials and applied them to the field of X-ray indirect detection. Rb_2CuCl_3 demonstrated an appreciable light yield of 16,600 photons per MeV and large and linear scintillation response within a range from 48.6 nGy_{air}/s to 15.7 μGy_{air}/s. In 2021, Zhang et al. [62] prepared a large-area (25 cm^2) $CsCu_2I_3$ scintillator film with good scintillation properties by oriented

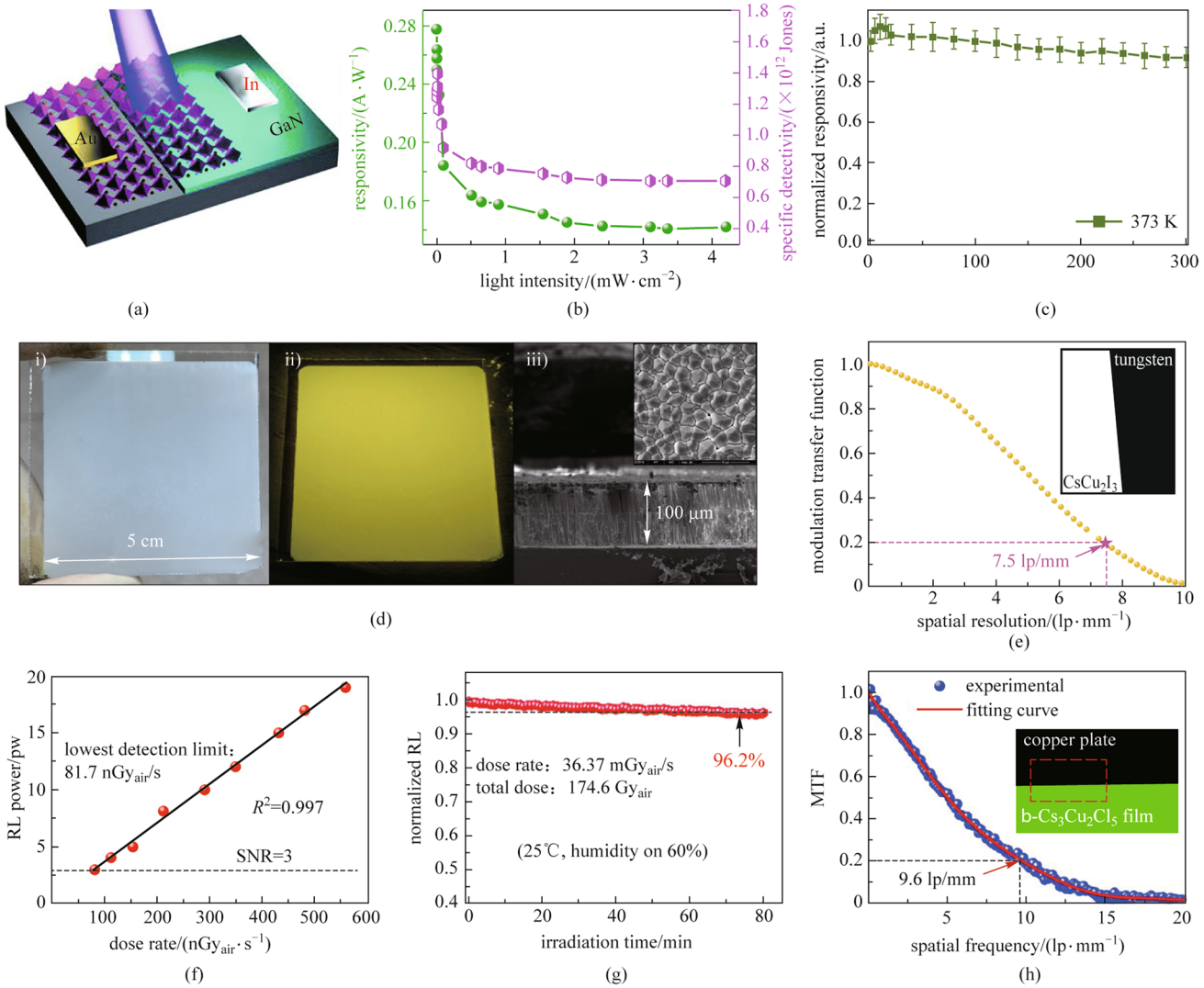

Fig. 5 **a** Schematic illustration of the $Cs_3Cu_2I_5$/GaN heterojunction device; **b** Responsivity and specific detectivity of the photodetector versus light intensity; **c** Responsivity evolution of the heterojunction photodetector monitored at 373 K in ambient air. **a**–**c** Reprinted with permission from Ref. [59], Copyright 2020, Royal Society of Chemistry; **d** $CsCu_2I_3$ film for the X-ray imaging application: (i) Optical photograph, (ii) photoluminescent photograph, and (iii) SEM image of oriented structured $CsCu_2I_3$ thick film; **e** Modulation transfer function (MTF) of the $CsCu_2I_3$ detector, measured by the slanted-edge method (inset). **d**, **e** Reprinted with permission from Ref. [62], Copyright 2021, American Chemical Society; **f** Lowest detection limit of $Cs_3Cu_2Cl_5$ films at signal noise ratio (SNR) of 3; **g** Operational stability of $Cs_3Cu_2Cl_5$ films by continuous X-ray irradiation; **h** MTF of $Cs_3Cu_2Cl_5$ films. **f**–**h** Reprinted with permission from Ref. [64], Copyright 2021, Royal Society of Chemistry

structural design as shown in Fig. 5d. $CsCu_2I_3$ films with a columnar crystal shape were found to effectively reduce light scattering and improve X-ray imaging quality. This $CsCu_2I_3$ scintillator achieved a high spatial resolution of 7.5 lp/mm in X-ray imaging as shown in Fig. 5e. There are two factors that affect the quality of X-ray imaging: light yield and light scattering. The light yield depends on how well the material itself responds to X-rays. The effect of light scattering can be largely reduced by structural design. In 2021, Zhao et al. [63] prepared a high-performance scintillator by combining $Cs_3Cu_2I_5$ with anodic aluminum oxide (AAO). As $Cs_3Cu_2I_5$ was confined in a hollow columnar structure formed by the AAO, light scattering was significantly reduced and the imaging quality was further improved. The $Cs_3Cu_2I_5$–AAO scintillator demonstrated high spatial resolution (10.4 lp/mm at modulation transfer function (MTF) = 0.2). In 2021, Zhou et al. [64] prepared $Cs_3Cu_2Cl_5$ nanocrystal thin films by a spin coating method. The scintillator film had a light yield of 34,000 ± 4000 photons per MeV, a spatial resolution of 9.6 lp/mm in X-ray imaging (Fig. 5h), and a minimum detection limit of 81.7 nGy_{air}/s (Fig. 5f). In addition, the scintillator exhibited excellent environmental and irradiation stability as shown in Fig. 5g. Flexible X-ray scintillators are a key problem in the field of X-ray detection. In the medical

field, flexible scintillators allow for more detailed and clear imaging, enabling doctors to make more accurate judgments about the pathological tissue. In 2022, Han et al. [55] tuned the crystal structure and optical properties of $Cs_3Cu_2Cl_5$ by doping K^+ and enhanced the PLQY of $Cs_3Cu_2Cl_5$ nanosheet to 81.39%. They prepared large-area flexible scintillator films by combining this doped nanosheet with polystyrene. The flexible scintillator film exhibited a very sensitive scintillation response to X-ray signals within 20–160 keV. This work provides a new idea for future preparation and research of flexible scintillator materials.

Light yield is a particularly important parameter in evaluating the performance of scintillator materials. Metal ion doping has shown significant advantages in increasing the light yield of scintillators. Wang et al. [65] optimized the optical properties of $Cs_3Cu_2I_5$ by doping In^+ and prepared $Cs_3Cu_2I_5$:In^+ single crystals by the vertical Bridgman method. In^+ doping enhanced the PLQY of $Cs_3Cu_2I_5$ from 68.1 to 88.4%. Benefiting from the higher PLQY, $Cs_3Cu_2I_5$:In^+ can achieve a superior light yield of 53,000 photons per MeV, which is comparable to commercial CsI:Tl single crystals (54,000 photons per MeV). Li et al. [66] prepared $Cs_3Cu_2I_5$:Mn^+ scintillator material, and the light yield was enhanced to 67,000 photons per MeV due to the introduction of new luminescence centers by Mn^+ doping, which reduced the non-radiative complex of $Cs_3Cu_2I_5$ and overcame the temperature quenching effect of the intrinsic material. Rare earth elements have been intensively investigated in doping engineering. Cheng et al. [67] prepared the Tl-doped $Cs_3Cu_2I_5$ crystals with excellent optical properties, exhibiting a high PLQY of 79.2% and the light yield of 87,000 photons per MeV. Optical yield largely determines the imaging quality of scintillator materials. Copper-based metal halides show excellent optical yield performance with the optimization of ion doping engineering, proving their potential advantages in the field of scintillator materials.

Although copper-based metal halides have achieved some success in the field of X-ray scintillators and photodetection, there are still some problems, such as the low resolution of X-ray imaging, and difficulty in achieving large-area high-quality flexible films.

5 Conclusions and perspectives

We have reviewed the developments in the field of copper-based metal halides in recent years and summarized their development status and problems in terms of crystal structure/morphology, photophysics/optical properties and applications. Although copper-based metal halides have achieved excellent results in many areas, there are still many new opportunities and challenges:

1) Mechanism. Copper-based metal halides possess excellent optical properties due to their unique crystal structure and low electronic dimension. The luminescence properties of this class of materials were found to be derived from STE, and there are still many problems in the study of the luminescence principles of STE. Further studies on the relationship between photoexcitation, crystal structure changes, and excited state reorganization are still needed;
2) Stability. Copper-based metal halides are soft lattice materials that undergo lattice deformation when excited by UV light. There are relatively few studies on how the lattice deformation is restored and whether the lattice deformation affects the stability of the material. Therefore, the study of the lattice stability of copper-based metal halides is a significant direction. If the material stability problem can be solved, they will realize more in-depth applications in the field of X-ray detection;
3) Fabrication. The current research on all-inorganic copper-based metal halides is mainly focused on material preparation. The preparation cycle of single crystal materials is too long and the production efficiency is low. In addition, it is difficult to prepare thin films by a solution method due to the insolubility of raw materials, and the quality of quantum dot films needs to be further improved. The search for new preparation processes is the biggest issue at present. The vacuum evaporation method has shown great advantages with insoluble materials and the films prepared by this method are of good quality, uniformity and flatness. The raw materials of copper-based metal halides are also insoluble, so the development of a vacuum vapor deposition method for the preparation of fully inorganic copper-based metal halides is also a worthy research direction.

Acknowledgements This work was funded by the National Natural Science Foundation of China (Grant Nos. 22279049 and 52073131), and the Fundamental Research Funds for the Central Universities (Nos. lzujbky-2021-ct15 and lzujbky-2021-sp69).

Author contributions ZJ conceived the idea, crafted and guided the entire dissertation writing process. FQ and YL co-wrote the manuscript. All authors read and approved the final manuscript.

Declarations

Competing interests The authors declare that they have no competing interests.

References

1. Liang, J., Liu, J., Jin, Z.: All-inorganic halide perovskites for optoelectronics: progress and prospects. Solar RRL **1**(10), 1700086 (2017)
2. Xiang, W., Tress, W.: Review on recent progress of all-inorganic metal halide perovskites and solar cells. Adv. Mater. **31**(44), e1902851 (2019)
3. Chen, W., Li, X., Li, Y., Li, Y.: A review: Crystal growth for high-performance all-inorganic perovskite solar cells. Energy Environ. Sci. **13**(7), 1971–1996 (2020)
4. Yuan, J., Hazarika, A., Zhao, Q., Ling, X., Moot, T., Ma, W., Luther, J.M.: Metal halide perovskites in quantum dot solar cells: progress and prospects. Joule **4**(6), 1160–1185 (2020)
5. Liu, P., Han, N., Wang, W., Ran, R., Zhou, W., Shao, Z.: High-quality ruddlesden-popper perovskite film formation for high-performance perovskite solar cells. Adv. Mater. **33**(10), e2002582 (2021)
6. Park, N.G.: Perovskite solar cells: an emerging photovoltaic technology. Mater. Today **18**(2), 65–72 (2015)
7. Leijtens, T., Bush, K.A., Prasanna, R., Mcgehee, M.D.: Opportunities and challenges for tandem solar cells using metal halide perovskite semiconductors. Nat. Energy **3**(10), 828–838 (2018)
8. Wu, T., Qin, Z., Wang, Y., Wu, Y., Chen, W., Zhang, S., Cai, M., Dai, S., Zhang, J., Liu, J., Zhou, Z., Liu, X., Segawa, H., Tan, H., Tang, Q., Fang, J., Li, Y., Ding, L., Ning, Z., Qi, Y., Zhang, Y., Han, L.: The main progress of perovskite solar cells in 2020–2021. Nano-Micro Lett. **13**(1), 152 (2021)
9. Li, B., Li, Z., Wu, X., Zhu, Z.: Interface functionalization in inverted perovskite solar cells: from material perspective. Nano Res Energy **1**, e9120011 (2022)
10. Tan, Z.K., Moghaddam, R.S., Lai, M.L., Docampo, P., Higler, R., Deschler, F., Price, M., Sadhanala, A., Pazos, L.M., Credgington, D., Hanusch, F., Bein, T., Snaith, H.J., Friend, R.H.: Bright light-emitting diodes based on organometal halide perovskite. Nat. Nanotechnol. **9**(9), 687–692 (2014)
11. Liu, M., Wan, Q., Wang, H., Carulli, F., Sun, X., Zheng, W., Kong, L., Zhang, Q., Zhang, C., Zhang, Q., Brovelli, S., Li, L.: Suppression of temperature quenching in perovskite nanocrystals for efficient and thermally stable light-emitting diodes. Nat. Photonics **15**(5), 379–385 (2021)
12. Ji, K., Anaya, M., Abfalterer, A., Stranks, S.D.: Halide perovskite light-emitting diode technologies. Adv. Opt. Mater. **9**(18), 2002128 (2021)
13. Dou, L., Yang, Y.M., You, J., Hong, Z., Chang, W.H., Li, G., Yang, Y.: Solution-processed hybrid perovskite photodetectors with high detectivity. Nat. Commun. **5**(1), 5404 (2014)
14. Ramasamy, P., Lim, D.H., Kim, B., Lee, S.H., Lee, M.S., Lee, J.S.: All-inorganic cesium lead halide perovskite nanocrystals for photodetector applications. Chem. Commun. (Camb.) **52**(10), 2067–2070 (2016)
15. Wang, H.P., Li, S., Liu, X., Shi, Z., Fang, X., He, J.H.: Low-dimensional metal halide perovskite photodetectors. Adv. Mater. **33**(7), e2003309 (2021)
16. Li, Z., Peng, G., Chen, H., Shi, C., Li, Z., Jin, Z.: Metal-free PAZE-$NH_4X_3{\cdot}H_2O$ perovskite for flexible transparent X-ray detection and imaging. Angew. Chem. Int. Ed. **61**(36), 202207198 (2022)
17. Chen, Q., Wu, J., Ou, X., Huang, B., Almutlaq, J., Zhumekenov, A.A., Guan, X., Han, S., Liang, L., Yi, Z., Li, J., Xie, X., Wang, Y., Li, Y., Fan, D., Teh, D.B.L., All, A.H., Mohammed, O.F., Bakr, O.M., Wu, T., Bettinelli, M., Yang, H., Huang, W., Liu, X.: All-inorganic perovskite nanocrystal scintillators. Nature **561**(7721), 88–93 (2018)
18. Cao, F., Yu, D., Ma, W., Xu, X., Cai, B., Yang, Y.M., Liu, S., He, L., Ke, Y., Lan, S., Choy, K.L., Zeng, H.: Shining emitter in a stable host: design of halide perovskite scintillators for X-ray imaging from commercial concept. ACS Nano **14**(5), 5183–5193 (2020)
19. Zhu, W., Ma, W., Su, Y., Chen, Z., Chen, X., Ma, Y., Bai, L., Xiao, W., Liu, T., Zhu, H., Liu, X., Liu, H., Liu, X., Yang, Y.M.: Low-dose real-time X-ray imaging with nontoxic double perovskite scintillators. Light Sci. Appl. **9**(1), 112 (2020)
20. Chen, H., Wang, Q., Peng, G., Wang, S., Lei, Y., Wang, H., Yang, Z., Sun, J., Li, N., Zhao, L., Lan, W., Jin, Z.: Cesium lead halide nanocrystals based flexible X-ray imaging screen and visible dose rate indication on paper substrate. Adv. Opt. Mater. **10**(8), 2102790 (2022)
21. Dong, H., Zhang, C., Liu, X., Yao, J., Zhao, Y.S.: Materials chemistry and engineering in metal halide perovskite lasers. Chem. Soc. Rev. **49**(3), 951–982 (2020)
22. Zhang, Q., Shang, Q., Su, R., Do, T.T.H., Xiong, Q.: Halide perovskite semiconductor lasers: materials, cavity design, and low threshold. Nano Lett. **21**(5), 1903–1914 (2021)
23. Li, Z., Zhou, F., Yao, H., Ci, Z., Yang, Z., Jin, Z.: Halide perovskites for high-performance X-ray detector. Mater. Today **48**, 155–175 (2021)
24. Zhou, F., Li, Z., Lan, W., Wang, Q., Ding, L., Jin, Z.: Halide perovskite, a potential scintillator for X-ray detection. Small Methods **4**(10), 2000506 (2020)
25. Krishnamoorthy, T., Ding, H., Yan, C., Leong, W.L., Baikie, T., Zhang, Z., Sherburne, M., Li, S., Asta, M., Mathews, N., Mhaisalkar, S.G.: Lead-free germanium iodide perovskite materials for photovoltaic applications. J. Mater. Chem. A Mater. Energy Sustain. **3**(47), 23829–23832 (2015)
26. Yu, B.B., Chen, Z., Zhu, Y., Wang, Y., Han, B., Chen, G., Zhang, X., Du, Z., He, Z.: Heterogeneous 2D/3D tin-halides perovskite solar cells with certified conversion efficiency breaking 14%. Adv. Mater. **33**(36), e2102055 (2021)
27. Jiang, F., Yang, D., Jiang, Y., Liu, T., Zhao, X., Ming, Y., Luo, B., Qin, F., Fan, J., Han, H., Zhang, L., Zhou, Y.: Chlorine-incorporation-induced formation of the layered phase for antimony-based lead-free perovskite solar cells. J. Am. Chem. Soc. **140**(3), 1019–1027 (2018)
28. Leng, M., Yang, Y., Zeng, K., Chen, Z., Tan, Z., Li, S., Li, J., Xu, B., Li, D., Hautzinger, M.P., Fu, Y., Zhai, T., Xu, L., Niu, G., Jin, S., Tang, J.: All-inorganic bismuth-based perovskite quantum dots with bright blue photoluminescence and excellent stability. Adv. Funct. Mater. **28**(1), 1704446 (2018)
29. Li, M., Li, F., Gong, J., Zhang, T., Gao, F., Zhang, W.H., Liu, M.: Advances in TiN(II)-based perovskite solar cells: from material physics to device performance. Small Struct. **3**(1), 2100102 (2022)
30. Tang, Y., Tang, S., Luo, M., Guo, Y., Zheng, Y., Lou, Y., Zhao, Y.: All-inorganic lead-free metal halide perovskite quantum dots: progress and prospects. Chem. Commun. (Camb.) **57**(61), 7465–7479 (2021)
31. Jun, T., Sim, K., Iimura, S., Sasase, M., Kamioka, H., Kim, J., Hosono, H.: Lead-free highly efficient blue-emitting $Cs_3Cu_2I_5$ with 0D electronic structure. Adv. Mater. **30**(43), e1804547 (2018)
32. Cao, L., Liu, X., Li, Y., Li, X., Du, L., Chen, S., Zhao, S., Wang, C.: Recent progress in all-inorganic metal halide nanostructured

perovskites: materials design, optical properties, and application. Front. Phys. **16**(3), 33201 (2021)
33. Hull, S., Berastegui, P.: Crystal structures and ionic conductivities of ternary derivatives of the silver and copper monohalides—II: ordered phases within the $(AgX)_x(MX)_{1-x}$ and $(CuX)_x(MX)_{1-x}$ (M=K, Rb and Cs; X=Cl, Br and I) systems. J. Solid State Chem. **177**(9), 3156–3173 (2004)
34. Li, Y., Zhou, Z., Tewari, N., Ng, M., Geng, P., Chen, D., Ko, P.K., Qammar, M., Guo, L., Halpert, J.E.: Progress in copper metal halides for optoelectronic applications. Mater. Chem. Front. **5**(13), 4796–4820 (2021)
35. Grandhi, G.K., Viswanath, N.S.M., Cho, H.B., Han, J.H., Kim, S.M., Choi, S., Im, W.B.: Mechanochemistry as a green route: Synthesis, thermal stability, and postsynthetic reversible phase transformation of highly-luminescent cesium copper halides. J. Phys. Chem. Lett. **11**(18), 7723–7729 (2020)
36. Lin, R., Guo, Q., Zhu, Q., Zhu, Y., Zheng, W., Huang, F.: All-inorganic CsCu2I3 single crystal with high-PLQY (approximately 15.7%) intrinsic white-light emission via strongly localized 1D excitonic recombination. Adv. Mater. **31**(46), e1905079 (2019)
37. Yang, B., Yin, L., Niu, G., Yuan, J.H., Xue, K.H., Tan, Z., Miao, X.S., Niu, M., Du, X., Song, H., Lifshitz, E., Tang, J.: Lead-free halide Rb2CuBr 3 as sensitive X-ray scintillator. Adv. Mater. **31**(44), e1904711 (2019)
38. Sun, X.J., Xia, M.L., Xu, Y.S., Tang, J., Niu, G.D.: Research progress of perovskite direct X-ray imaging. Chinese J. Luminescence **43**(7), 1014–1026 (2022)
39. Xu, Y., Li, Y., Wang, Q., Chen, H., Lei, Y., Feng, X., Ci, Z., Jin, Z.: Two-dimensional BA_2PbBr 4-based wafer for X-rays imaging application. Mater. Chem. Front. **6**(10), 1310–1316 (2022)
40. Zeng, J., Bi, L., Cheng, Y., Xu, B., Jen, A.K.Y.: Self-assembled monolayer enabling improved buried interfaces in blade-coated perovskite solar cells for high efficiency and stability. Nano Res Energy **1**, e9120004 (2022)
41. Zhang, F., Zhao, Z., Chen, B., Zheng, H., Huang, L., Liu, Y., Wang, Y., Rogach, A.L.: Strongly emissive lead-free 0D $Cs_3Cu_2I_5$ perovskites synthesized by a room temperature solvent evaporation crystallization for down-conversion light-emitting devices and fluorescent inks. Adv. Opt. Mater. **8**(8), 1901723 (2020)
42. Lin, R., Zhu, Q., Guo, Q., Zhu, Y., Zheng, W., Huang, F.: Dual self-trapped exciton emission with ultrahigh photoluminescence quantum yield in $CsCu_2I_3$ and $Cs_3Cu_2I_5$ perovskite single crystals. J. Phys. Chem. C **124**(37), 20469–20476 (2020)
43. Zhou, Z., Li, Y., Xing, Z., Sung, H.H.Y., Williams, I.D., Li, Z., Wong, K.S., Halpert, J.E.: Rapid synthesis of bright, shape-controlled, large single crystals of $Cs_3Cu_2X_5$ for phase pure single (X=Br, Cl) and mixed halides (X=Br, Cl) as the blue and green components for printable white light-emitting devices. Adv. Mater. Interfaces **8**(20), 2101471 (2021)
44. Mo, X., Li, T., Huang, F., Li, Z., Zhou, Y., Lin, T., Ouyang, Y., Tao, X., Pan, C.: Highly-efficient all-inorganic lead-free 1D $CsCu_2I_3$ single crystal for white-light emitting diodes and UV photodetection. Nano Energy **81**, 105570 (2021)
45. Zhao, X., Niu, G., Zhu, J., Yang, B., Yuan, J.H., Li, S., Gao, W., Hu, Q., Yin, L., Xue, K.H., Lifshitz, E., Miao, X., Tang, J.: All-inorganic copper halide as a stable and self-absorption-free X-ray scintillator. J. Phys. Chem. Lett. **11**(5), 1873–1880 (2020)
46. Yang, J., Kang, W., Liu, Z., Pi, M., Luo, L.B., Li, C., Lin, H., Luo, Z., Du, J., Zhou, M., Tang, X.: High-performance deep ultraviolet photodetector based on a one-dimensional lead-free halide perovskite $CsCu_2I_3$ film with high stability. J. Phys. Chem. Lett. **11**(16), 6880–6886 (2020)
47. Ma, Z., Shi, Z., Qin, C., Cui, M., Yang, D., Wang, X., Wang, L., Ji, X., Chen, X., Sun, J., Wu, D., Zhang, Y., Li, X.J., Zhang, L., Shan, C.: Stable yellow light-emitting devices based on ternary copper halides with broadband emissive self-trapped excitons. ACS Nano **14**(4), 4475–4486 (2020)
48. Roccanova, R., Yangui, A., Nhalil, H., Shi, H., Du, M.H., Saparov, B.: Near-unity photoluminescence quantum yield in blue-emitting $Cs_3Cu_2Br_{5-x}I_x$ ($0 \le x \le 5$). ACS Appl. Electron. Mater. **1**(3), 269–274 (2019)
49. Xie, L., Chen, B., Zhang, F., Zhao, Z., Wang, X., Shi, L., Liu, Y., Huang, L., Liu, R., Zou, B., Wang, Y.: Highly luminescent and stable lead-free cesium copper halide perovskite powders for UV-pumped phosphor-converted light-emitting diodes. Photon. Res. **8**(6), 768–775 (2020)
50. Cheng, P., Sun, L., Feng, L., Yang, S., Yang, Y., Zheng, D., Zhao, Y., Sang, Y., Zhang, R., Wei, D., Deng, W., Han, K.: Colloidal synthesis and optical properties of all-inorganic low-dimensional cesium copper halide nanocrystals. Angew. Chem. Int. Ed. **58**(45), 16087–16091 (2019)
51. Li, Y., Vashishtha, P., Zhou, Z., Li, Z., Shivarudraiah, S.B., Ma, C., Liu, J., Wong, K.S., Su, H., Halpert, J.E.: Room temperature synthesis of stable, printable $Cs_3Cu_2X_5$ (X = I, Br/I, Br, Br/Cl, Cl) colloidal nanocrystals with near-unity quantum yield green emitters (X = Cl). Chem. Mater. **32**(13), 5515–5524 (2020)
52. Luo, Z., Li, Q., Zhang, L., Wu, X., Tan, L., Zou, C., Liu, Y., Quan, Z.: 0D $Cs_3Cu_2X_5$ (X = I, Br, and Cl) nanocrystals: colloidal syntheses and optical properties. Small **16**(3), e1905226 (2020)
53. Zhao, S., Chen, C., Cai, W., Li, R., Li, H., Jiang, S., Liu, M., Zang, Z.: Efficiently luminescent and stable lead-free $Cs_3Cu_2Cl_5$@silica nanocrystals for white light-emitting diodes and communication. Adv. Opt. Mater. **9**(13), 2100307 (2021)
54. Zhang, R., Mao, X., Zheng, D., Yang, Y., Yang, S., Han, K.: A lead-free all-inorganic metal halide with near-unity green luminescence. Laser Photonics Rev. **14**(5), 2000027 (2020)
55. Han, L., Sun, B., Guo, C., Peng, G., Chen, H., Yang, Z., Li, N., Ci, Z., Jin, Z.: Photophysics in zero-dimensional potassium-doped cesium copper chloride Cs3Cu2Cl5 nanosheets and its application for high-performance flexible X-ray detection. Adv. Opt. Mater. **10**(6), 2102453 (2022)
56. Zhang, B., Wu, X., Zhou, S., Liang, G., Hu, Q.: Self-trapped exciton emission in inorganic copper(I) metal halides. Front Optoelectron. **14**(4), 459–472 (2021)
57. Du, M.H.: Emission trend of multiple self-trapped excitons in luminescent 1D copper halides. ACS Energy Lett. **5**(2), 464–469 (2020)
58. Zhang, Z.X., Li, C., Lu, Y., Tong, X.W., Liang, F.X., Zhao, X.Y., Wu, D., Xie, C., Luo, L.B.: Sensitive deep ultraviolet photodetector and image sensor composed of inorganic lead-free $Cs_3Cu_2I_5$ perovskite with wide bandgap. J. Phys. Chem. Lett. **10**(18), 5343–5350 (2019)
59. Li, Y., Shi, Z., Liang, W., Wang, L., Li, S., Zhang, F., Ma, Z., Wang, Y., Tian, Y., Wu, D., Li, X., Zhang, Y., Shan, C., Fang, X.: Highly stable and spectrum-selective ultraviolet photodetectors based on lead-free copper-based perovskites. Mater. Horiz. **7**(2), 530–540 (2020)
60. Li, Y., Shi, Z., Wang, L., Chen, Y., Liang, W., Wu, D., Li, X., Zhang, Y., Shan, C., Fang, X.: Solution-processed one-dimensional $CsCu_2I_3$ nanowires for polarization-sensitive and flexible ultraviolet photodetectors. Mater. Horiz. **7**(6), 1613–1622 (2020)
61. Ma, J., Xia, X., Yan, S., Li, Y., Liang, W., Yan, J., Chen, X., Wu, D., Li, X., Shi, Z.: Stable and self-powered solar-blind ultraviolet photodetectors based on a $Cs_3Cu_2I_5/\beta$-Ga_2O_3 heterojunction prepared by dual-source vapor codeposition. ACS Appl. Mater. Interfaces **13**(13), 15409–15419 (2021)
62. Zhang, M., Zhu, J., Yang, B., Niu, G., Wu, H., Zhao, X., Yin, L., Jin, T., Liang, X., Tang, J.: Oriented-structured $CsCu_2I_3$ film by close-space sublimation and nanoscale seed screening for high-resolution X-ray imaging. Nano Lett. **21**(3), 1392–1399 (2021)

63. Zhao, X., Jin, T., Gao, W., Niu, G., Zhu, J., Song, B., Luo, J., Pan, W., Wu, H., Zhang, M., He, X., Fu, L., Li, Z., Zhao, H., Tang, J.: Embedding $Cs_3Cu_2I_5$ scintillators into anodic aluminum oxide matrix for high-resolution X-ray imaging. Adv. Opt. Mater. **9**(24), 2101194 (2021)
64. Zhou, Q., Ren, J., Xiao, J., Lei, L., Liao, F., Di, H., Wang, C., Yang, L., Chen, Q., Yang, X., Zhao, Y., Han, X.: Highly efficient copper halide scintillators for high-performance and dynamic X-ray imaging. Nanoscale **13**(47), 19894–19902 (2021)
65. Wang, Q., Zhou, Q., Nikl, M., Xiao, J., Kucerkova, R., Beitlerova, A., Babin, V., Prusa, P., Linhart, V., Wang, J., Wen, X., Niu, G., Tang, J., Ren, G., Wu, Y.: Highly resolved X-ray imaging enabled by In(I) doped perovskite-like $Cs_3Cu_2Cl_5$ single crystal scintillator. Adv. Opt. Mater. **10**(11), 2200304 (2022)
66. Li, X., Chen, J., Yang, D., Chen, X., Geng, D., Jiang, L., Wu, Y., Meng, C., Zeng, H.: Mn^{2+} induced significant improvement and robust stability of radioluminescence in $Cs_3Cu_2I_5$ for high-performance nuclear battery. Nat. Commun. **12**(1), 3879 (2021)
67. Cheng, S., Nikl, M., Beitlerova, A., Kucerkova, R., Du, X., Niu, G., Jia, Y., Tang, J., Ren, G., Wu, Y.: Ultrabright and highly efficient all-inorganic zero-dimensional perovskite scintillators. Adv. Opt. Mater. **9**(13), 2100460 (2021)

Fu Qiu received his B.S. degree from Tianjin University of Technology, China. He is currently a M.S. student under the supervision of Prof. Zhiwen Jin. His research interests are copper metal halide materials based X-ray detectors.

Yutian Lei received his B.S. degree from Jiangxi University of Science and Technology and M.S. degree from Lanzhou University, China. He is currently a Ph.D. student at Lanzhou University. His research focuses on the application of low-dimensional metal halide in the field of X-ray detection.

Zhiwen Jin is a professor at the School of Physical Science and Technology, Lanzhou University, China. He received the B.S. degree from Lanzhou University in 2011 and the Ph.D. degree from the Institute of Chemistry, Chinese Academy of Sciences, China in 2016. He has been listed as the "Clarivate Highly Cited Researchers" and "Elsevier Most Cited Chinese Researchers." His research interests include metal halide materials based X-ray detectors, device physic, and integration method.